Forward Charm Production

R. Vogt

Lawrence Livermore National Laboratory, Livermore, CA 94551, USA
Physics and Astronomy Department, UC Davis, Davis, CA 95616, USA

based on:
RV, arXiv:2101.02858, Phys. Rev. C 103, 035204 (2021)
RV, arXiv:2207.04347
RV, in progress

Figure 1: This work was performed under the auspices of the U.S. Department of Energy by Lawrence Livermore National Laboratory under Contract DE-AC52-07NA27344 and the LLNL-LDRD Program under Project No. 21-LW-034.

Outline

- **Introduction to Intrinsic Charm**
- **Charm Production in Perturbative QCD, Including Cold Nuclear Matter**
- **Total Production in $p + p$ and $p + \mathrm{Pb}$**
- **Comparison to Previous Fixed-Target J/ψ Production**
- **Summary**

Intrinsic Charm in the Proton

What is Intrinsic Charm?

Intrinsic charm in the proton $|uudc\overline{c}\rangle$, was first proposed by in the 1980's

Charm hadrons that can be produced directly from this state by coalesence of the quarks in the state: $J/\psi(c\overline{c})$, $\Lambda_c(udc)$, $\Sigma_c^{++}(uuc)$, $\Sigma_c^{+}(udc)$, $\Sigma_c^{0}(ddc)$, $\overline{D}^0(\overline{c}u)$, $D^-(\overline{c}d)$. These are "leading" charm; other states that need to be produced by higher Fock states, like $|uudc\overline{c}q\overline{q}\rangle$, are "non-leading" charm.

If this state dominates the wavefunction, the charm quarks carry a larger fraction of the hadron momentum, enhancing charm production in the forward x_F region

A number of experimental hints have been seen, no conclusive results

- **Charm structure function, F_2^c, large at largest x and highest Q^2 measured (EMC)**
- **Leading charm asymmetries consistent with intrinsic charm predictions (D^- over D^+ in $\pi^- p$ interactions, E791)**
- **Double J/ψ production observed at high pair x_F by NA3**
- **Forward charm production observed in many fixed-target experiments (WA82, WA89, E791, SELEX and others)**
- **Proposed explanation of high energy astrophysical neutrino rate at Ice Cube (Brodsky and Laha)**

Global PDF analyses have tried incorporating intrinsic charm and reported a range of possible contributions from 0 to 1%

LHCb: Evidence of Intrinsic Charm in $Z + c$-Jet Events

$Z+c$-jet ratio to Z+all-jet events at $\sqrt{s} = 13$ TeV is more consistent with calculations including intrinsic charm at high $y(Z)$, up to 1% intrinsic charm content

Differences between calculations without intrinsic charm (no IC) and intrinsic charm allowed calculations, either with NNPDF 3.0 including IC or CT14 with a 1% IC content, grows larger with increasing $y(Z)$

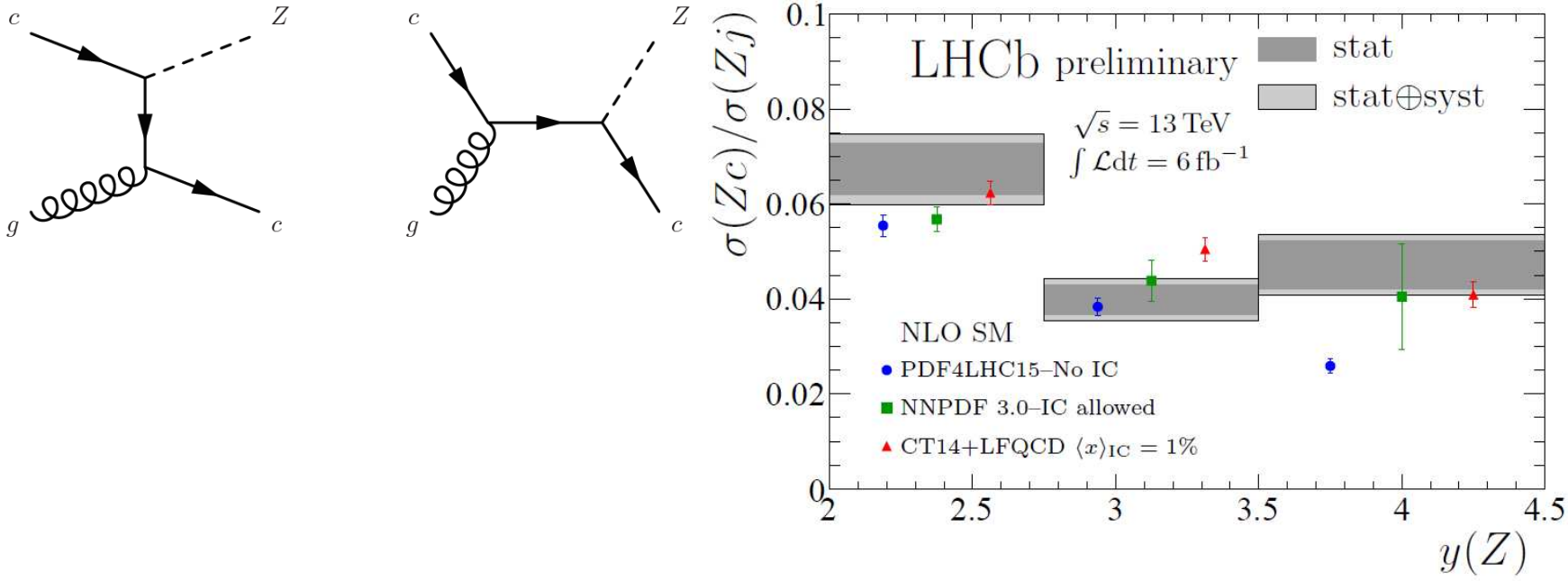

Figure 2: (Left) Leading order diagrams producing $Z + c$-jet events. (Right) Ratio of $Z + c$-jets to Z+all-jet events from LHCb. Images from https://lhcb-public.web.cern.ch/Welcome.html#IC, 27 July 2021.

Intrinsic Charm

Probability distribution of five-particle Fock state of the proton:

$$dP_{\mathrm{ic}\,5} = P^0_{\mathrm{ic}\,5} N_5 \int dx_1 \cdots dx_5 \int dk_{x\,1} \cdots dk_{x\,5} \int dk_{y\,1} \cdots dk_{y\,5} \frac{\delta(1-\sum_{i=1}^5 x_i)\delta(\sum_{i=1}^5 k_{x\,i})\delta(\sum_{i=1}^5 k_{y\,i})}{(m_p^2 - \sum_{i=1}^5 (\widehat{m}_i^2/x_i))^2}$$

$i = 1,2,3$ are u, u, d light quarks, 4 and 5 are c and $\overline{c}$, N_t normalizes the integral to unity and P^0_{ic} scales the normalized probability to the assumed intrinsic charm content: 0.1%, 0.31% and 1%, representing the range of probabilities assumed previously. The distributions for J/ψ and $\overline{D}$ are calculated assuming coalesence via delta functions.

The IC cross section is determined from soft interaction scale breaking coherence of the Fock state, $\mu^2 = 0.1$ GeV^2

$$\sigma_{\mathrm{ic}}(pp) = P_{\mathrm{ic}\,5} \sigma^{\mathrm{in}}_{pN} \frac{\mu^2}{4\widehat{m}_c^2}$$

The J/ψ cross section from intrinsic charm is then obtained by multiplying by the normalization factor for the CEM to the J/ψ

$$\sigma^{J/\psi}_{\mathrm{ic}}(pp) = F_C \sigma_{\mathrm{ic}}(pp)$$

The A dependence is

$$\sigma^{J/\psi}_{\mathrm{ic}}(pA) = \sigma^{J/\psi}_{\mathrm{ic}}(pp)\, A^{\beta}$$

where $\beta = 0.71$ for $p + A$ (NA3); cross sections for $\overline{D}$ are similar except $F_C \equiv 1$

Intrinsic Charm x_F and p_T Distributions

Peak of the J/ψ x_F distribution is forward, away from midrapidity

p_T distribution is harder than the pQCD distribution at low energy; at higher energies and $x_F \sim 0$, the pQCD contribution will drown the intrinsic charm contribution

The p_T distribution also depends on range of k_T integrations

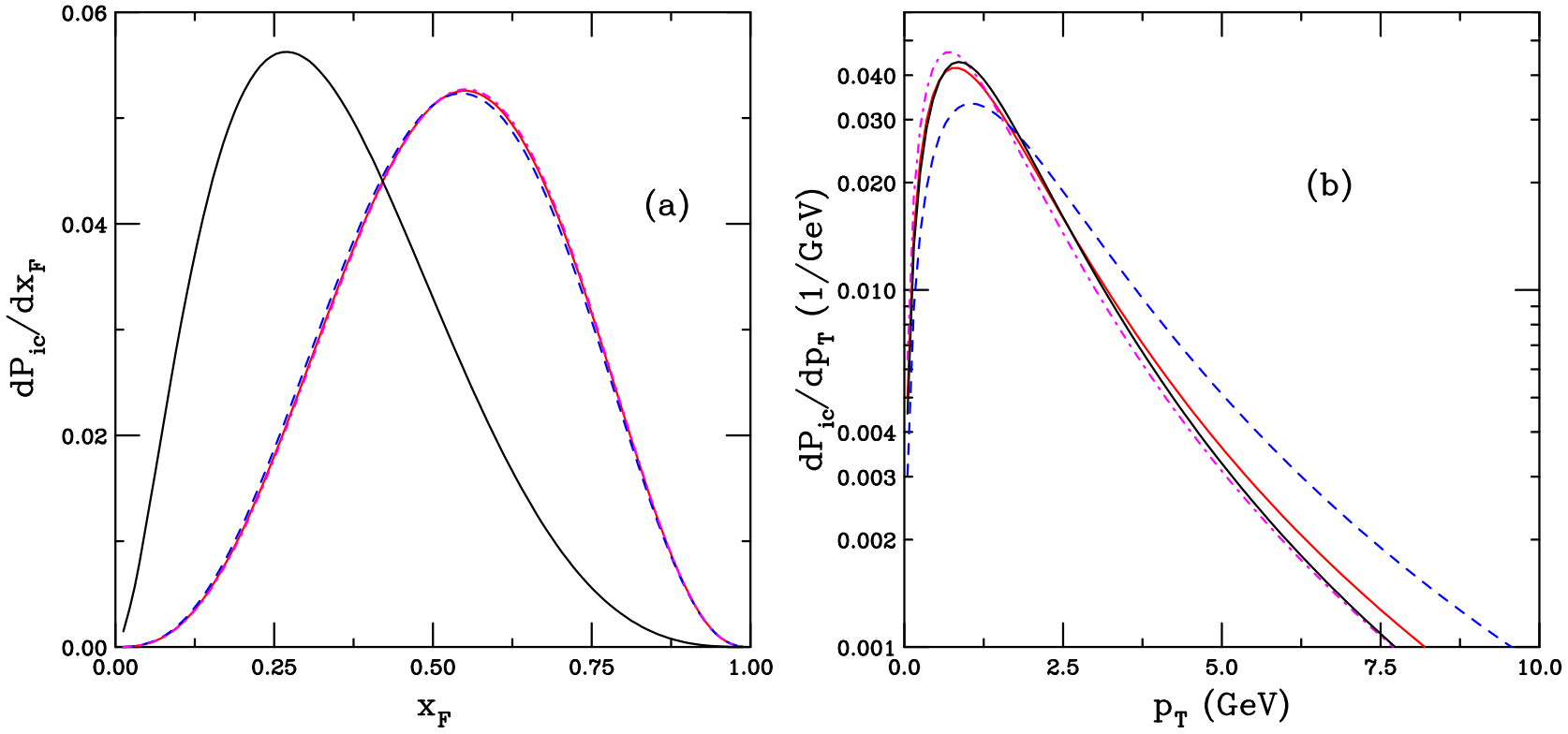

Figure 3: The probability distributions for J/ψ production from a five-particle proton Fock state as a function of x_F (a) and p_T (b). The results are shown for different values of the k_T range for the light and charm quarks. The red curve employs the default values, $k_q^{\max} = 0.2$ GeV and $k_c^{\max} = 1.0$ GeV while the blue dashed curve increases $k_q^{\max}$ and $k_c^{\max}$ by a factor of two and the dot-dashed magenta curve employs half the values of $k_q^{\max}$ and $k_c^{\max}$. The solid black curve shows the x and p_T distributions for a single charm quark from the state.

Intrinsic Charm y Distribution Depends on $\sqrt{s_{NN}}$

Once the x_F distribution is transformed to rapidity, it becomes sensitive to $\sqrt{s_{NN}}$ since $x_F = (2m_T/\sqrt{s_{NN}}) \sinh y$

As $\sqrt{s_{NN}}$ increases, the intrinsic charm rapidity distribution is moved further away from midrapidity, at $\sqrt{s_{NN}} = 7$ TeV it is inaccessible to most forward detectors

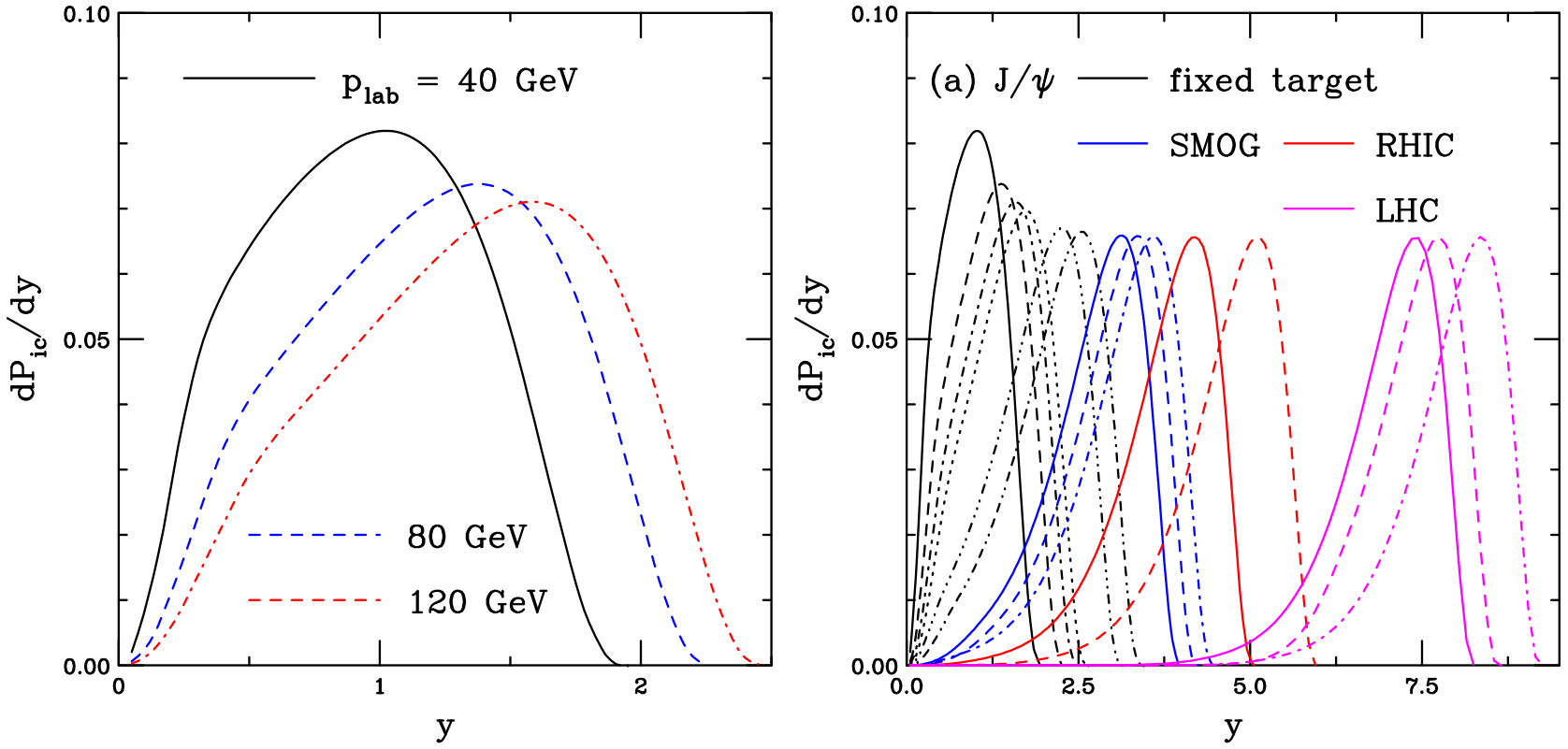

Figure 4: The probability distributions for J/ψ production from a five-particle proton Fock state as a function of y. The results are shown for different values of $\sqrt{s_{NN}}$. The solid black curve shows $\sqrt{s_{NN}} = 8.8$ GeV, the blue dashed curve is for $\sqrt{s_{NN}} = 12.3$ GeV, and the red dot-dashed curve is for $\sqrt{s_{NN}} = 15.4$ GeV. The results in (b) include energies up to $\sqrt{s_{NN}} = 13$ TeV.

IC y Dependence on $k_T^{\max}$, m_i at $\sqrt{s_{NN}} = 15.4$ GeV

Left-hand plot shows the results of doubling and halving the k_T integration range of all constituents; doubling the range shifts it backward, halving it moves it forward

Right-hand plot shows the results of increasing m_c from 1.27 GeV to 1.5 GeV and, with $m_c = 1.27$ GeV, reducing the constituent m_q from 0.3 GeV to 0.02 GeV, increasing m_c shifts y distribution to lower y, reducing m_q moves it further forward

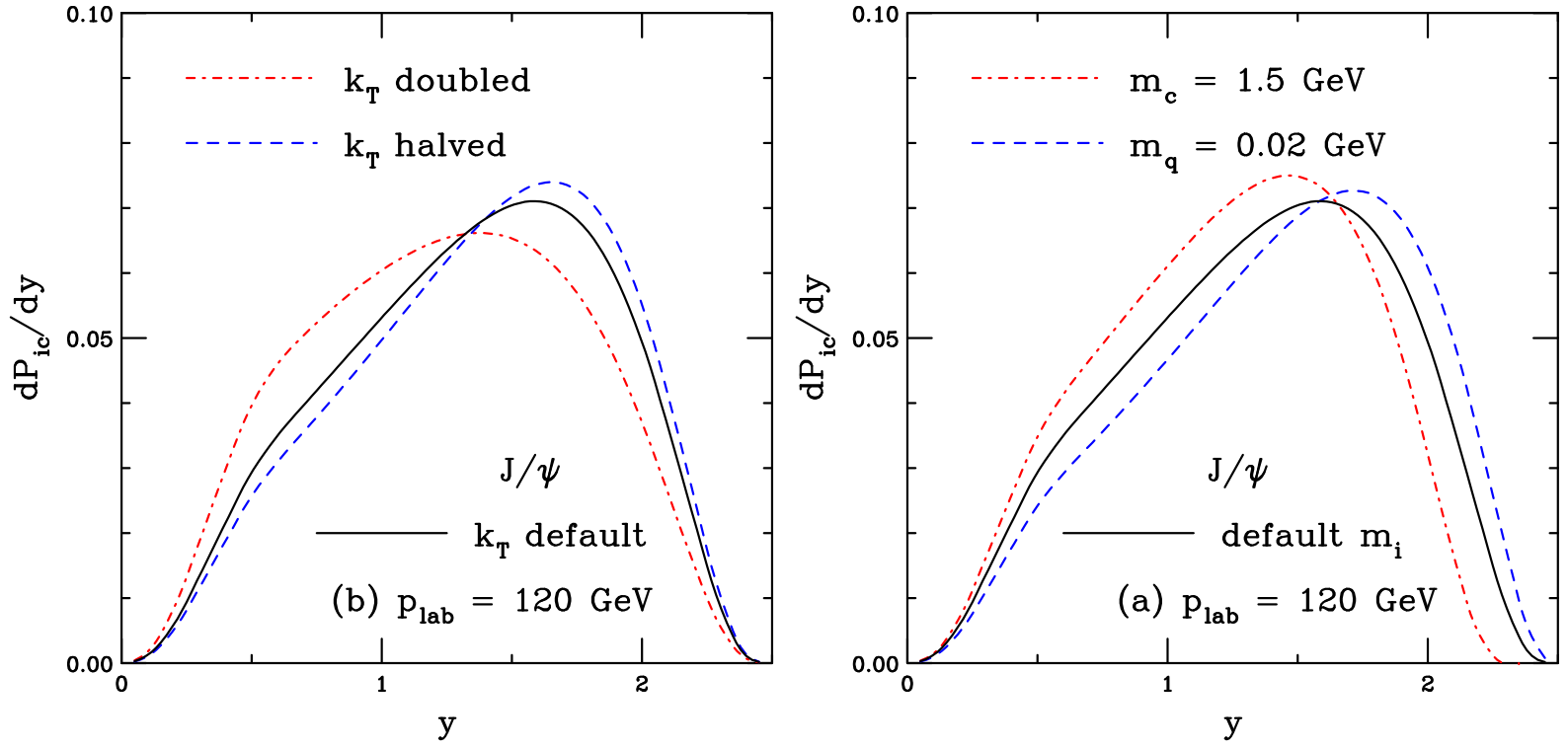

Figure 5: The probability distributions for J/ψ production from a five-particle proton Fock state as a function of y for $\sqrt{s_{NN}} = 15.4$ GeV. The dot-dashed red curve employs the default values, $k_q^{\max} = 0.2$ GeV and $k_c^{\max} = 1.0$ GeV in both plots. On the left-hand side, the black solid curve shown the results for $k_q^{\max}$ and $k_c^{\max}$ increased by a factor of two while the blue dashed curve employs half the values of $k_q^{\max}$ and $k_c^{\max}$. On the right-hand side. the solid black curve shows the result for increasing m_c to 1.5 GeV, the dashed blue curve shows the result for lowering m_q to 0.02 GeV.

y Dependence of IC p_T Distributions

The p_T distributions are shown for several energies when the rapidity range is restricted to $0 < y < 1$, green curve shows integration over all y

The p_T distribution at midrapidity is shifted to higher p_T and integral in this range decreases as $\sqrt{s_{NN}}$ increases: at higher energies and midrapidity, there is no contribution from intrinsic charm at low p_T

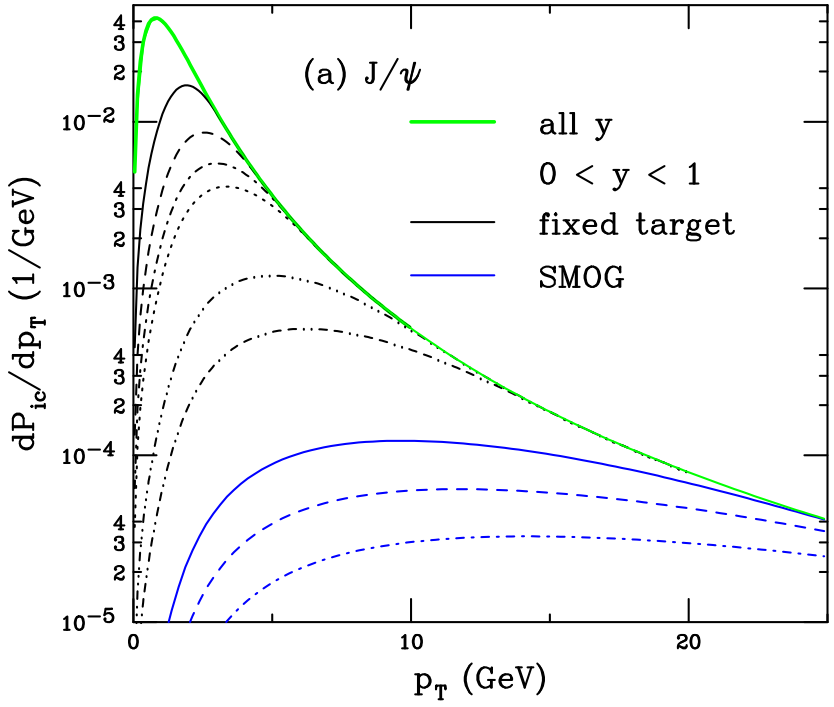

Figure 6: The probability distributions for J/ψ production from a five-particle proton Fock state as a function of p_T. The results are shown for all rapidity in the solid green curve. Results for restricting the rapidity range to $0 < y < 1$ are shown for $p_{\rm lab} = 40$, 80 and 120 GeV by the solid black, dashed blue and dot-dashed red respectively.

Charm Production in Perturbative QCD

Charmonium Production in the Color Evaporation Model

The CEM at NLO is employed for the perturbative production cross section:

$$\sigma_{\rm CEM}(pp) = F_C \sum_{i,j} \int_{4m^2}^{4m_H^2} d\hat{s} \int dx_1\, dx_2\ F_i^p(x_1, \mu_F^2, k_{T_1})\ F_j^p(x_2, \mu_F^2, k_{T_2})\ \hat{\sigma}_{ij}(\hat{s}, \mu_F^2, \mu_R^2)$$

Parton densities factorized into longitudinal (CT10) and a k_T-dependent component to implement k_T broadening a la low p_T resummation

$$F^p(x, \mu_F^2, k_T) = f^p(x, \mu_F^2) G_p(k_T)$$

$$G_p(k_T) \ = \ \frac{1}{\pi \langle k_T^2 \rangle_p} \exp(-k_T^2/\langle k_T^2 \rangle_p)$$

$$\langle k_T^2 \rangle_p = \left[1 + \frac{1}{n} \ln \left(\frac{\sqrt{s_{NN}}({\rm GeV})}{20\,{\rm GeV}} \right) \right]\ {\rm GeV}^2$$

$\langle k_T^2 \rangle_p$ broadening assumed energy dependent, $n = 12$ from J/ψ data

$0.72 \leq \langle k_T^2 \rangle_p \leq 1.49$ from $p_{\rm lab} = 40$ GeV to $\sqrt{s_{NN}} = 5$ TeV

Open charm production, $\sigma_{\rm OHF}$, is similar but $F_C \equiv 1$ and upper limit of integral is $\hat{s} \to s$

Uncertainty band on cross section set by:

$$\frac{d\sigma_{\rm max}}{dX} \ = \ \frac{d\sigma_{\rm cent}}{dX} + \sqrt{\left(\frac{d\sigma_{\mu,{\rm max}}}{dX} - \frac{d\sigma_{\rm cent}}{dX} \right)^2 + \left(\frac{d\sigma_{m,{\rm max}}}{dX} - \frac{d\sigma_{\rm cent}}{dX} \right)^2}$$

$$\frac{d\sigma_{\rm min}}{dX} \ = \ \frac{d\sigma_{\rm cent}}{dX} - \sqrt{\left(\frac{d\sigma_{\mu,{\rm min}}}{dX} - \frac{d\sigma_{\rm cent}}{dX} \right)^2 + \left(\frac{d\sigma_{m,{\rm min}}}{dX} - \frac{d\sigma_{\rm cent}}{dX} \right)^2}$$

J/ψ Distributions in CEM at $\sqrt{s_{NN}} = 15.4$ GeV

Uncertainty bands defined by $(m, \mu_F/m_T, \mu_R/m_T) = (1.27 \pm 0.09\,\mathrm{GeV}, 2.1^{+2.55}_{-0.85}, 1.6^{+0.11}_{-0.12})$**;** μ_F**, factorization scale, and** μ_R**, renormalization scale, defined relative to pair transverse mass:** $\mu_{F,R} \propto m_T = \sqrt{m^2 + p_T^2}$ **where** $p_T^2 = 0.5(p_{T_Q}^2 + p_{T_{\overline{Q}}}^2)$

Scale uncertainties set by $\{(\mu_F/m_T, \mu_F/m_T)\} = \{(C,C),\ (H,H),\ (L,L),\ (C,L),\ (L,C),\ (C,H),\ (H,C)\}$ **(Mass uncertainties dominate.)**

Distributions are narrower at lower energies and harder at higher energies

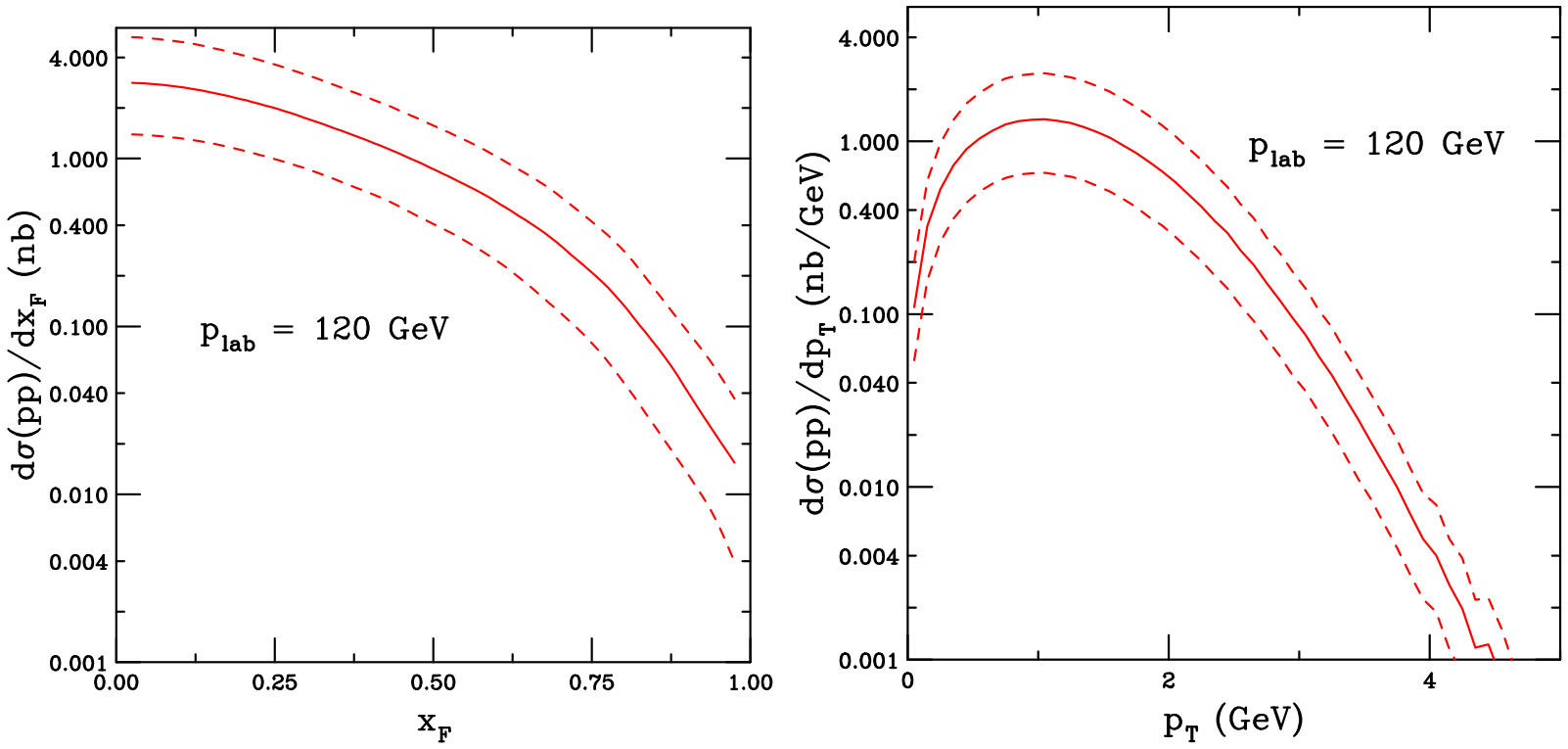

Figure 7: The J/ψ production cross sections in the CEM in $p+p$ collisions at $\sqrt{s} = 15.4$ GeV as a function of x_F (a) and p_T (b), integrated over all phase space, are shown. The solid curves show the central values while the dashed curves outline the upper and lower limits of the uncertainty band.

Cold Matter Effects on Perturbative Cross Section

The J/ψ production cross section in a $p+A$ collision in pQCD is

$$\sigma_{pA}^{J/\psi} = \sigma_{\rm CEM}(pA) = S_A^{\rm abs} F_C \sum_{i,j} \int_{4m^2}^{4m_H^2} ds \int dx_1\, dx_2\ F_i^p(x_1, \mu_F^2, k_T)\ F_j^A(x_2, \mu_F^2, k_T)\ \hat{\sigma}_{ij}(\hat{s}, \mu_F^2, \mu_R^2)$$

Survival probability for absorption of a (proto)charmonium state in nuclear matter:

$$\begin{aligned}
\sigma_{pA} = \sigma_{pN} S_A^{\rm abs} &= \sigma_{pN} \int d^2b \int_{-\infty}^{\infty} dz\, \rho_A(b,z) S^{\rm abs}(b) \\
&= \sigma_{pN} \int d^2b \int_{-\infty}^{\infty} dz\, \rho_A(b,z) \exp\left\{ - \int_z^{\infty} dz' \rho_A(b,z') \sigma_{\rm abs}(z'-z) \right\}
\end{aligned}$$

The absorption cross section is assumed constant. Prior fixed-target experiments extracted an effective absorption cross section from A^α analysis with $\alpha = 1 - 9\sigma_{\rm abs}/(16\pi r_0^2)$ assuming no other nuclear effects

Nuclear parton densities

$$\begin{aligned}
F_j^A(x_2, \mu_F^2, k_T) &= R_j(x_2, \mu_F^2, A) f_j(x_2, \mu_F^2) G_A(k_T) \\
F_i^p(x_1, \mu_F^2, k_T) &= f_i(x_1, \mu_F^2) G_p(k_T)
\end{aligned}$$

$G_A(k_T)$ includes increased broadening in the nuclear target ($A > 2$)

No absorption is assumed for $\overline{D}$ production

k_T Broadening in Nuclei

k_T broadening in nuclei may be enhanced through multiple scattering in the target; to implement enhanced broadening, a larger value of $\langle k_T^2 \rangle$ is used for nuclear targets

$$\langle k_T^2 \rangle_A = \langle k_T^2 \rangle_p + \delta k_T^2$$

δk_T^2 gives strength of broadening

$$\delta k_T^2 = (\langle \nu \rangle - 1)\Delta^2(\mu)$$

The broadening strength depends on the interaction scale:

$$\Delta^2(\mu) = 0.225 \frac{\ln^2(\mu/\mathrm{GeV})}{1 + \ln(\mu/\mathrm{GeV})} \mathrm{GeV}^2 \qquad \mu = 2m_c$$

Strength also depends on number of scatterings proton undergoes passing through nuclear target, $\langle \nu \rangle - 1$

$$\langle \nu \rangle = \sigma_{pp}^{\mathrm{in}} \frac{\int d^2b T_A^2(b)}{\int d^2b T_A(b)} = \frac{3}{2} \rho_0 R_A \sigma_{pp}^{\mathrm{in}}$$

T_A is the nuclear profile function, here $\rho_0 = 0.16/\mathrm{fm}^3$, $R_A = 1.2A^{1/3}$, and the inelastic $p + p$ cross section is $\sigma_{pp}^{\mathrm{in}} \sim 30$ mb for the energies considered here

Assuming a Pb target, $\delta k_T^2 = 0.41$ GeV^2, giving an average broadening in the nucleus of $\langle k_T^2 \rangle_A = 1.12$ GeV^2 at $p_{\mathrm{lab}} = 40$ and 1.9 GeV^2 at $\sqrt{s_{NN}} = 5$ TeV. Lighter mass targets would give smaller δk_T^2 and reduced additional broadening in nuclei

Nuclear Modification of the Parton Densities

EPPS16 nuclear parton density modifications differentiate between u and d valence quarks and all sea quarks; 20 parameters give 40 error sets + 1 central set

Uncertainties are determined by calculating cross section for each A with all error sets, adding differences around central set for each parameter in quadrature

Lower energies probe higher x, for $0 < y < 1$, the momentum fraction in the nucleus is in the antishadowing and EMC regions (see right-hand plot)

$$f_j^A(x_2, \mu_F^2) = R_j(x_2, \mu_F^2, A) f_j^p(x_2, \mu_F^2)$$

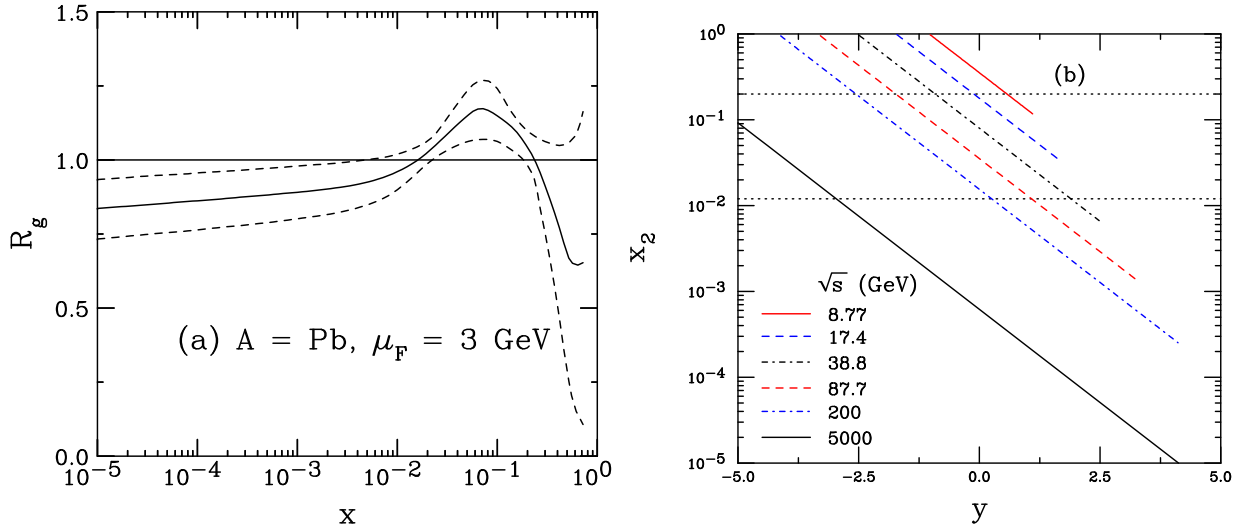

Figure 8: (Left) The EPPS16 ratio for a lead nucleus, with uncertainties, is shown at the scale of the J/ψ mass for gluons as a function of momentum fraction x. The central set is denoted by the solid curves while the dashed curves give the upper and lower limits of the uncertainty bands. (Right) The x_2 range as a function of rapidity for six values of $\sqrt{s_{NN}}$ covering a range of energies using nuclear targets: 8.77 (solid red), 17.4 (dashed blue), 38.8 (dot-dashed black), 87.7 (dashed red), 200 (dot-dashed blue) and 5000 (solid black) GeV. The upper and lower dotted lines at $x_2 = 0.012$ and 0.2 represent the lower and upper limits of the antishadowing region for $\mu_F = 3$ GeV.

Interplay of Shadowing and Absorption Affects $\sigma_{\rm abs}$

Depending on x values probed, shadowing can enhance or reduce absorption cross section extracted from data analysis assuming only absorption

Absorption alone always gives less than linear A dependence ($\alpha < 1$)

For SPS energies, $17.3 \leq \sqrt{s_{NN}} \leq 29$ GeV, rapidity range covered is in EMC and antishadowing region, $\alpha > 1$ with no absorption

Adding shadowing to absorption in the SPS energy region requires a larger absorption cross section is needed to maintain agreement with data

For $\sqrt{s_{NN}} \geq 38$ GeV, x in shadowing regime, thus $\alpha < 1$ with shadowing alone in forward region, reducing needed absorption cross section to $\sigma_{\rm abs} \sim 0$ at the LHC

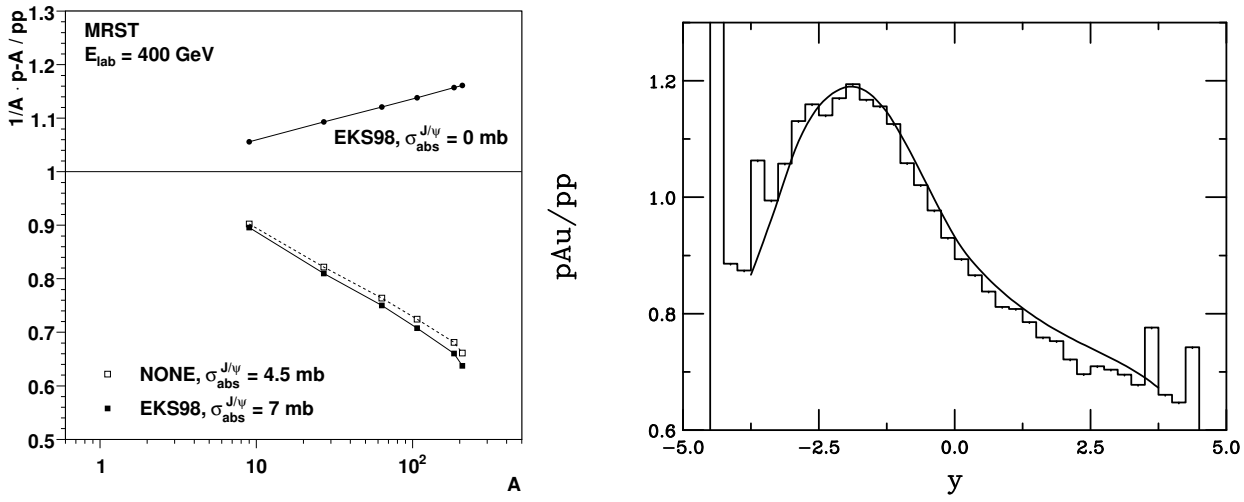

Figure 9: **(Left) Illustration of the interplay between shadowing and absorption. [C. Lourenco, H. K. Woehri and RV, JHEP 0902 (2009) 014.] (Right) Comparison of LO and NLO shadowing ratios.**

Energy Dependence of $\sigma_{\rm abs}^{J/\psi}$

At midrapidity, systematic decrease of $\sigma_{\rm abs}^{J/\psi}$ with $\sqrt{s_{NN}}$, independent of shadowing, trend continues at RHIC and above

$\sigma_{\rm abs}^{J/\psi}(y_{\rm cms}=0)$ at 158 GeV is significantly larger than that measured at 450 GeV

Calculations confirmed by NA60 pA measurements at 158 GeV showing stronger absorption with L than at 400 GeV, suggesting $\sigma_{\rm abs}^{J/\psi}=9$ mb at $\sqrt{s_{NN}}=15.4$ GeV, 5 mb at $\sqrt{s_{NN}}=38.8$ GeV, estimated $\sigma_{\rm abs}^{J/\psi}=11$, 10 mb at $\sqrt{s_{NN}}=12.3$, 8.8 GeV respectively

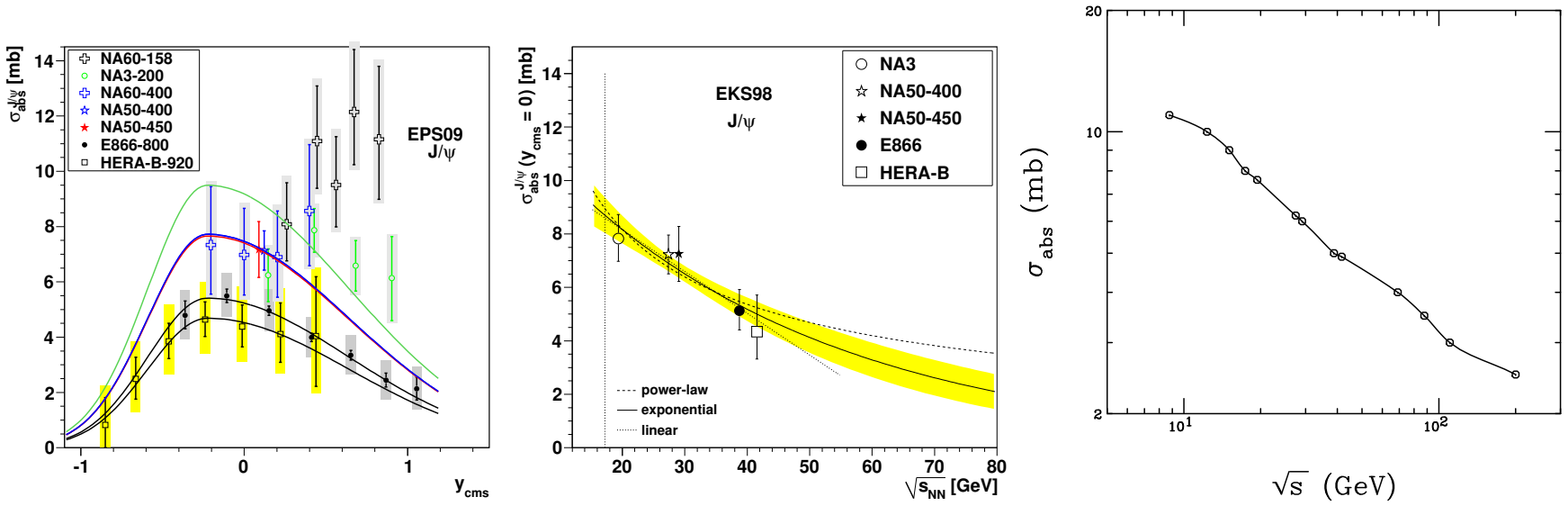

Figure 10: Left: Dependence of $\sigma_{\rm abs}^{J/\psi}$ on $y_{\rm cms}$ for all available data sets including EPS09 shadowing. The shape of the curves is fixed by the E866 and HERA-B data. [Lourenço, RV, Wöhri] Middle: The extracted energy dependence of $\sigma_{\rm abs}^{J/\psi}$ at midrapidity for power law (dashed), exponential (solid) and linear (dotted) approximations to $\sigma_{\rm abs}^{J/\psi}(y=0,\sqrt{s_{NN}})$ using the EKS98 shadowing parameterization with the CTEQ61L parton densities. The band around the exponential curve indicates the uncertainty in the extracted cross sections at $x_F\sim 0$ from NA3, NA50 at 400 and 450 GeV, E866 and HERA-B. The vertical dotted line indicates the energy of the Pb+Pb and In+In collisions at the CERN SPS. [Lourenço, RV, Wöhri] Right: The value of $\sigma_{\rm abs}$ as a function of $\sqrt{s_{NN}}$. The points show the energies used here. The line is meant to guide the eye.

Rapidity and p_T Distributions; J/ψ A Dependence

Model Calculation

Calculations shown here are for $p+p$ and $p+\mathrm{Pb}$, similar principle for $e+p$ and $e+A$ except, now, instead of soft gluons exchanged between two protons to disrupt state and bring it on shell, a soft photon can do the job

The same calculational structure holds for both J/ψ and $\overline{D}$ mesons

The $p+p$ and $p+\mathrm{Pb}$ distributions are shown at the same energy as a function of rapidity and transverse momentum; the nuclear suppression factor, $R_{p\mathrm{Pb}}$ is also shown

The nuclear suppression factor includes both the perturbative cross section and production by intrinsic charm:

$$\begin{aligned}
\sigma_{pA}^{J/\psi} &= \sigma_{\mathrm{CEM}}(pA) + \sigma_{\mathrm{ic}}^{J/\psi}(pA) \\
\sigma_{pp}^{J/\psi} &= \sigma_{\mathrm{CEM}}(pp) + \sigma_{\mathrm{ic}}^{J/\psi}(pp) \\
\sigma_{pA}^{\overline{D}} &= \sigma_{\mathrm{OHF}}(pA) + \sigma_{\mathrm{ic}}^{\overline{D}}(pA) \\
\sigma_{pp}^{\overline{D}} &= \sigma_{\mathrm{OHF}}(pp) + \sigma_{\mathrm{ic}}^{\overline{D}}(pp)
\end{aligned}$$

σ_{CEM} is the production cross section computed at NLO in the color evaporation model for $p+p$ and $p+A$ interactions, σ_{OHF} is the open heavy flavor cross section

$\sigma_{\mathrm{ic}}^{J/\psi}$ is intrinsic charm production cross section including the probability for an intrinsic charm contribution to the proton wavefunction

J/ψ $p+p$ distributions as a function of y and p_T: With and Without Intrinsic Charm

The strong energy dependence of the intrinsic charm contribution is evident; the pQCD contribution is overwhelmed at low energies but IC becomes negligible except for very forward rapidity at higher energies

Restricting the calculated p_T distributions to midrapidity significantly reduces the intrinsic charm contribution at low p_T, even for the lowest energies

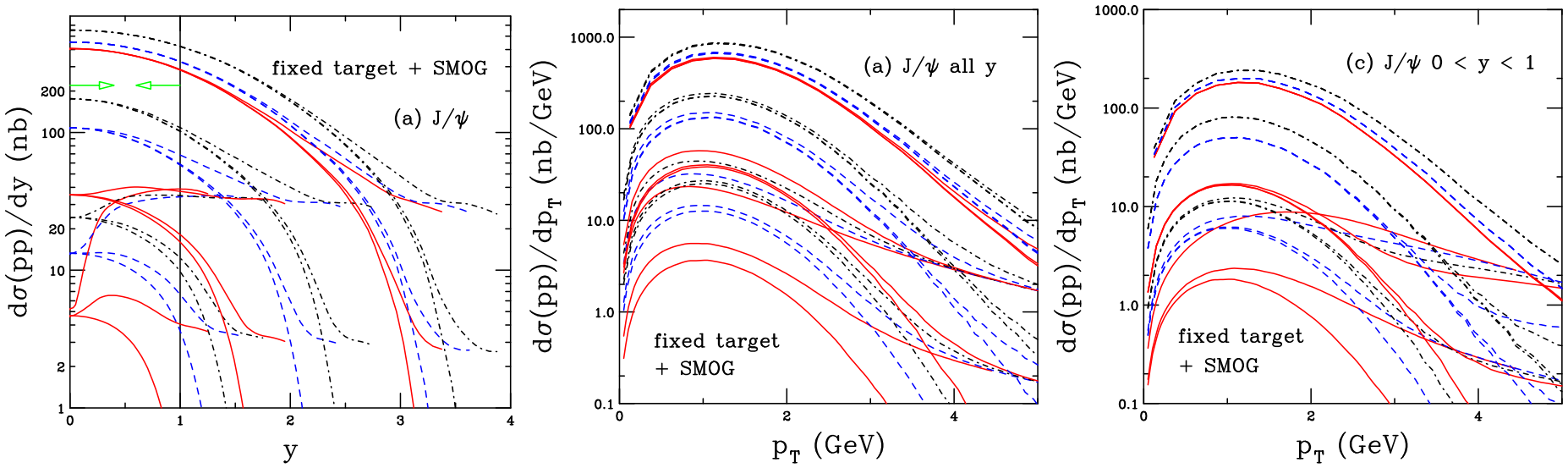

Figure 11: The combined distributions for J/ψ as a function of rapidity (left) and p_T (center and right), including both the perturbative QCD contribution and intrinsic charm from a $|uudc\overline{c}\rangle$ state. The calculated p_T distributions are integrated over all rapidity (middle) but limited to $0 < y < 1$ (right). Three curves are shown for each energy: no intrinsic charm (pQCD only); $P^0_{\rm ic\,5} = 0.1\%$; and $P^0_{\rm ic\,5} = 1\%$. The results are shown for fixed-target and SMOG energies, starting from $p_{\rm lab} = 40$ GeV (red solid), 80 GeV (blue dashed), 120 GeV (black dot-dashed), 158 GeV (red solid), 450 GeV (blue dashed), 800 GeV (black dot-dashed), $\sqrt{s} = 69$ GeV (solid red), 87.7 GeV (blue dashed) and 110.4 GeV (black dot-dashed). On the left, the vertical line with the green arrows shows the assumed rapidity acceptance of $0 < y < 1$.

$\overline{D}$ $p+p$ distributions as a function of y and p_T: With and Without Intrinsic Charm

Results are similar for $\overline{D}$ as for J/ψ, main difference is that the $\overline{D}$ distributions are somewhat broader while the p_T distributions have a slightly lower average p_T

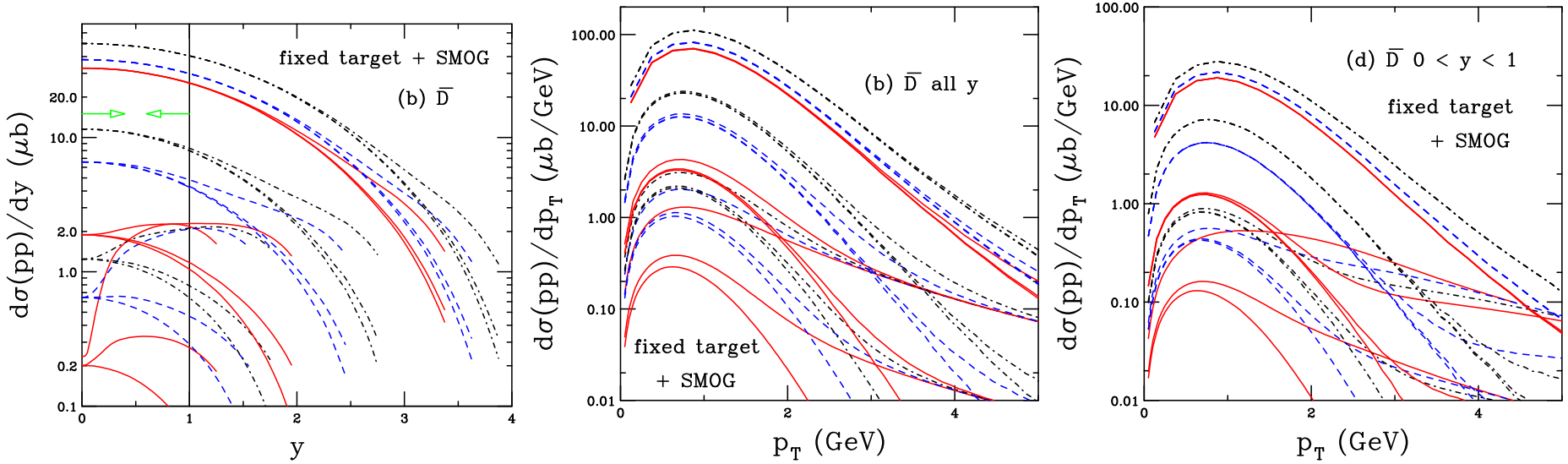

Figure 12: The combined distributions for $\overline{D}$ mesons as a function of rapidity (left) and p_T (center and right), including both the perturbative QCD contribution and intrinsic charm from a $|uudc\overline{c}\rangle$ state. The calculated p_T distributions are integrated over all rapidity (middle) but limited to $0 < y < 1$ (right). Three curves are shown for each energy: no intrinsic charm (pQCD only); $P^0_{\rm ic\,5} = 0.1\%$; and $P^0_{\rm ic\,5} = 1\%$. The results are shown for fixed-target and SMOG energies, starting from $p_{\rm lab} = 40$ GeV (red solid), 80 GeV (blue dashed), 120 GeV (black dot-dashed), 158 GeV (red solid), 450 GeV (blue dashed), 800 GeV (black dot-dashed), $\sqrt{s} = 69$ GeV (solid red), 87.7 GeV (blue dashed) and 110.4 GeV (black dot-dashed). On the left, the vertical line with the green arrows shows the assumed rapidity acceptance of $0 < y < 1$.

J/ψ $p+\mathrm{Pb}$ distributions as a function of y and p_T: Including Cold Nuclear Matter Effects

Here the p_T distribution is taken in the range $0 < |y| < 1$ for $p_{\mathrm{lab}} = 40$ and 800 GeV and $1.1 < |y| < 2.2$ for $\sqrt{s_{NN}} = 200$ GeV

An enhanced k_T broadening is assumed for $p+\mathrm{Pb}$ collisions

The A dependence of intrinsic charm suppresses its contribution in the lead nucleus

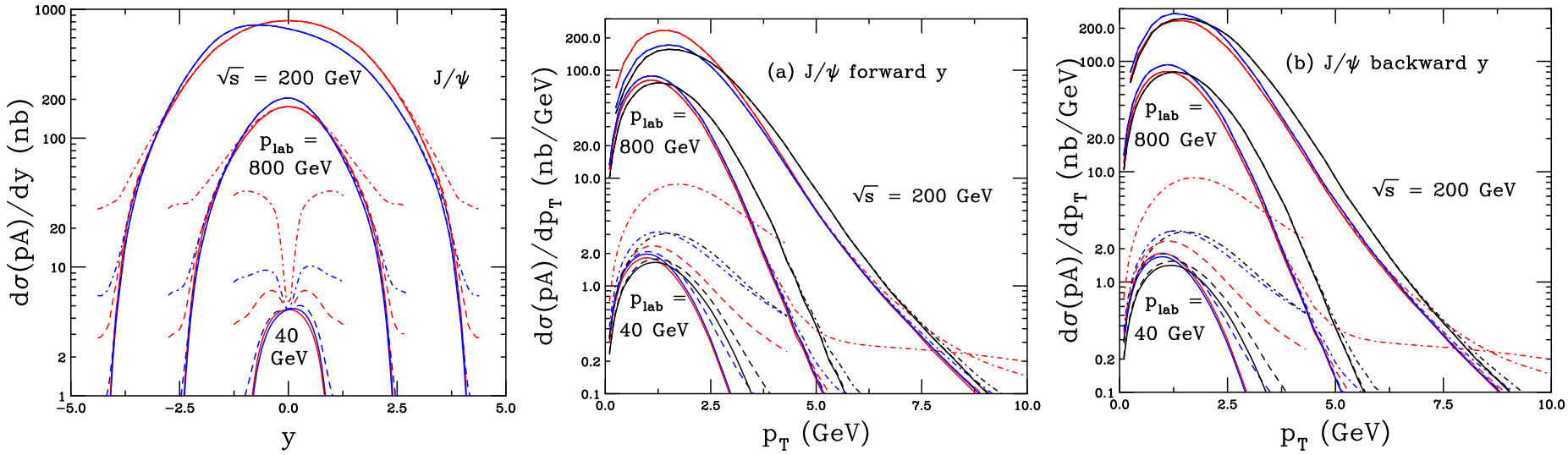

Figure 13: The J/ψ distributions at $p+p$ and $p+\mathrm{Pb}$ (per nucleon) at $p_{\mathrm{lab}} = 40$ and 800 GeV and $\sqrt{s} = 200$ GeV as a function of rapidity (left) and forward (middle, a) and backward (right, b) rapidity. The red curves show the results for $p+p$ collisions while the blue and black curves show the $p+\mathrm{Pb}$ distributions without and with an enhanced intrinsic k_T kick respectively. (The rapidity distributions are independent of the kick.) Three curves are shown in each case: no intrinsic charm (pQCD only, solid); $P^0_{\mathrm{ic}\,5} = 0.1\%$ (dashed); and $P^0_{\mathrm{ic}\,5} = 1\%$ (dot-dashed). No J/ψ absorption by nucleons is considered in the $p+\mathrm{Pb}$ calculation.

J/ψ Rapidity and p_T $p+\mathrm{Pb}$ Ratios: No Intrinsic Charm

Upper curves do not include absorption, lower curves employ $\sigma_{\mathrm{abs}} = 9$, 10 and 11 mb for $p_{\mathrm{lab}} = 120$, 80 and 40 GeV respectively

Rapidity distributions do not depend on k_T kick, only absorption, increasing beam energy broadens rapidity distribution, increasing absorption gives lower $R_{p\mathrm{Pb}}$

p_T distributions without k_T kick flat, higher incident energy goes further into anti-shadowing region, increasing energy also increases size of k_T kick

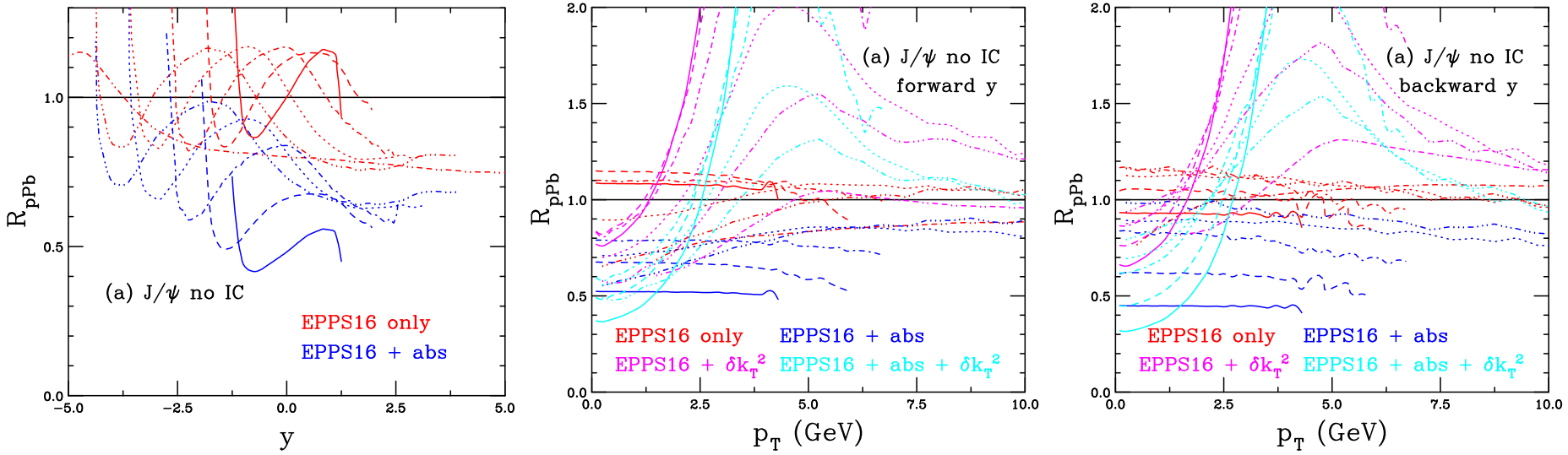

Figure 14: The nuclear modification factors for J/ψ production as a function of y (left) and p_T (right) for pQCD production alone for lead targets relative to proton. The rapidity distributions do not depend on the k_T broadening.

J/ψ $R_{p\mathrm{Pb}}$ as a function of y: With Intrinsic Charm

Upper curves do not include absorption, lower curves employ σ_{abs} from 11 mb for $p_{\mathrm{lab}} = 40$ GeV to 0 for $\sqrt{s_{NN}} = 5$ TeV

At these energies, $R_{p\mathrm{Pb}}$ is overwhelmed by intrinsic charm, even at midrapidity with $P^0_{\mathrm{ic}\,5} = 0.1\%$, unlike higher energy E866 results

At low center of mass energies, the rapidity distribution is not boosted very much. The energy dependence is quite strong.

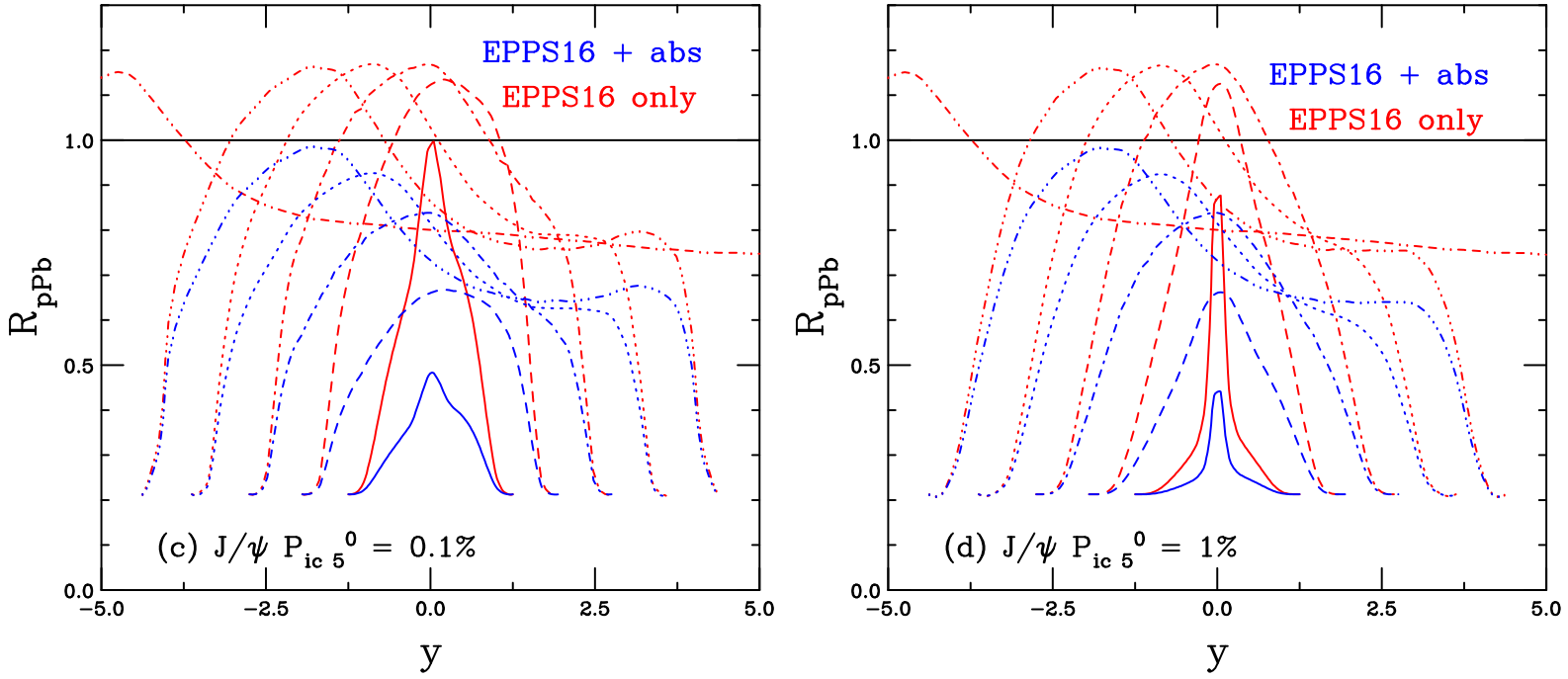

Figure 15: The nuclear suppression factor $R_{p\mathrm{Pb}}$ as a function of rapidity for J/ψ including both the perturbative QCD contribution and intrinsic charm from a five-particle proton Fock state with . The intrinsic charm contribution is varied in the panels from no intrinsic charm (pQCD only) (a) and (b); $P^0_{\mathrm{ic}\,5} = 0.1\%$ (left) $P^0_{\mathrm{ic}\,5} = 1\%$ (right). The red curves include EPPS16 modifications of the parton densities only while the blue curves include nuclear absorption of the J/ψ. The line types denote different energies: $p_{\mathrm{lab}} = 40$ GeV (solid), 158 GeV (dashes), 800 GeV (dot-dashed), $\sqrt{s} = 87.7$ GeV (dotted), 200 GeV (dot-dot-dot-dashed) and 5 TeV (dot-dot-dash-dashed). The rapidity distributions do not depend on k_T.

J/ψ $R_{p\mathrm{Pb}}$ as a function of p_T: With Intrinsic Charm

Upper curves do not include absorption, lower curves employ $\sigma_{\mathrm{abs}} = 9$, 10 and 11 mb for $p_{\mathrm{lab}} = 120$, 80 and 40 GeV respectively

Results are shown for forward rapidity only – the results are similar for backward rapidity and are not shown. The limiting A dependence with intrinsic charm is $A^{\beta-1} = 0.213$, reached at higher p_T with increasing energy

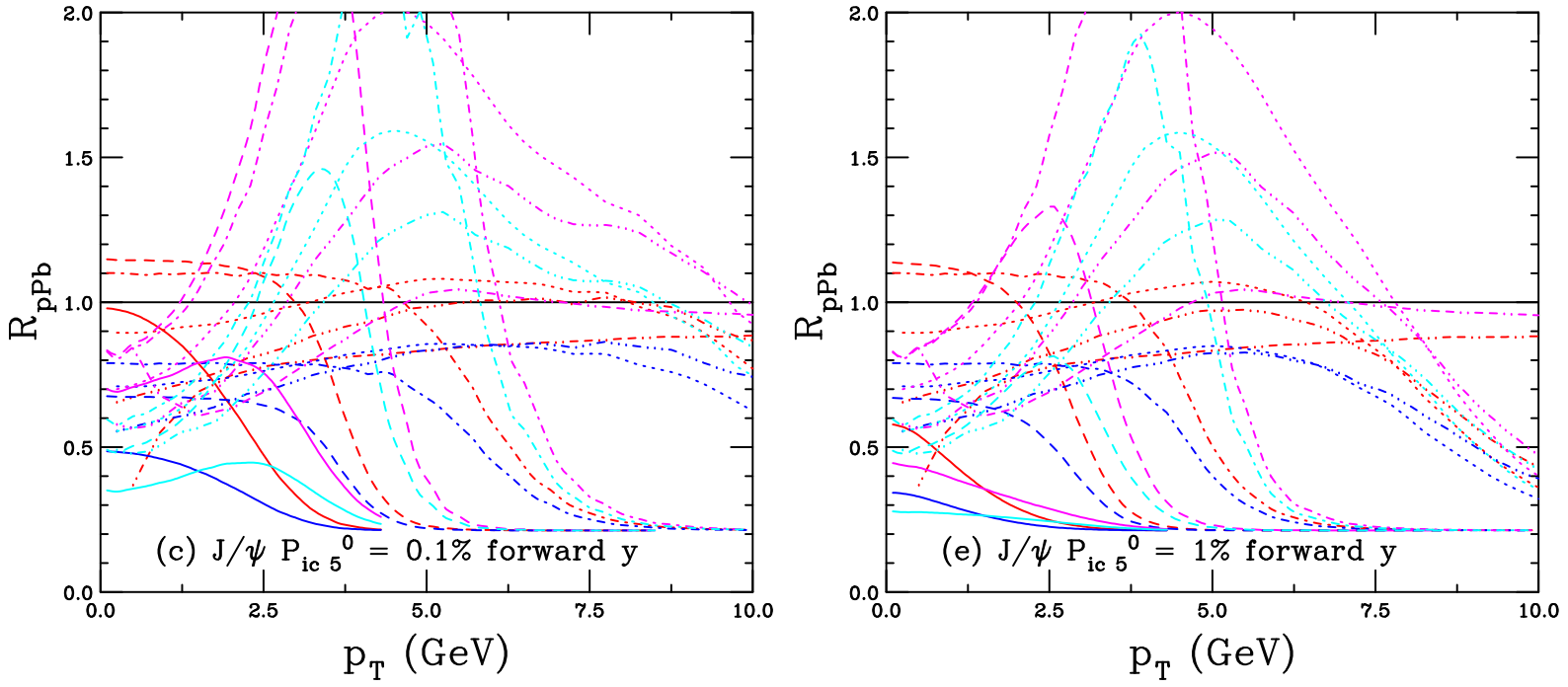

Figure 16: The nuclear modification factors for J/ψ production as a function of p_T for lead targets relative to proton with $P^0_{\mathrm{ic}\,5} = 0.1\%$ (left) and 1% (right). The red curves include the EPPS16 modifications of the parton densities only while the blue curves also include nuclear absorption of the J/ψ. The magenta curves include the EPPS16 modifications as well as k_T broadening while the cyan curves include EPPS16, nuclear absorption for the J/ψ, and k_T broadening. The line types denote different energies: $p_{\mathrm{lab}} = 40$ GeV (solid), 158 GeV (dashes), 800 GeV (dot-dashed), $\sqrt{s_{NN}} = 87.7$ GeV (dotted), 200 GeV (dot-dot-dot-dashed) and 5 TeV (dot-dot-dash-dashed). Note that the rapidity range is $0 < y < 1$ for all energies except the two highest where the rapidity range is $1.1 < y < 2.2$ for 200 GeV and $2.5 < y < 5$ for 5 TeV.

Comparison to Fixed-Target J/ψ Production

Summary of Previous Fixed-Target J/ψ Data

NA60 $p_{\rm lab} = 158$ **and 400 GeV, covering** $0.05 < x_F < 0.4$ **and** $-0.075 < x_F < 0.125$ **respectively, were taken on Be, Al, Cu, In, W, Pb, and U targets (PLB 706, 263 (2012))**

NA3 $p_{\rm lab} = 200$ **GeV,** $x_F > 0$**, taken on a Pt target (Z. Phys. C 20, 101 (1983))**

NA50 $p_{\rm lab} = 450$ **GeV, midrapidity** $(-0.1 < x_F < 0.1)$**, used Be, Al, Cu, Ag, W and Pb targets (EPJ C 33, 31 (2004))**

E866 $p_{\rm lab} = 800$ **GeV,** $-0.09 < x_F < 0.95$**, used Be, Fe, and W targets (PRL 84, 3256 (2000))**

HERA-B $p_{\rm lab} = 920$ **GeV,** $-0.34 < x_F < 0.14$**, used C, Ti and W targets (EPJ C 60, 525 (2009))**

E866 J/ψ x_F and p_T Distributions $(p+p)$

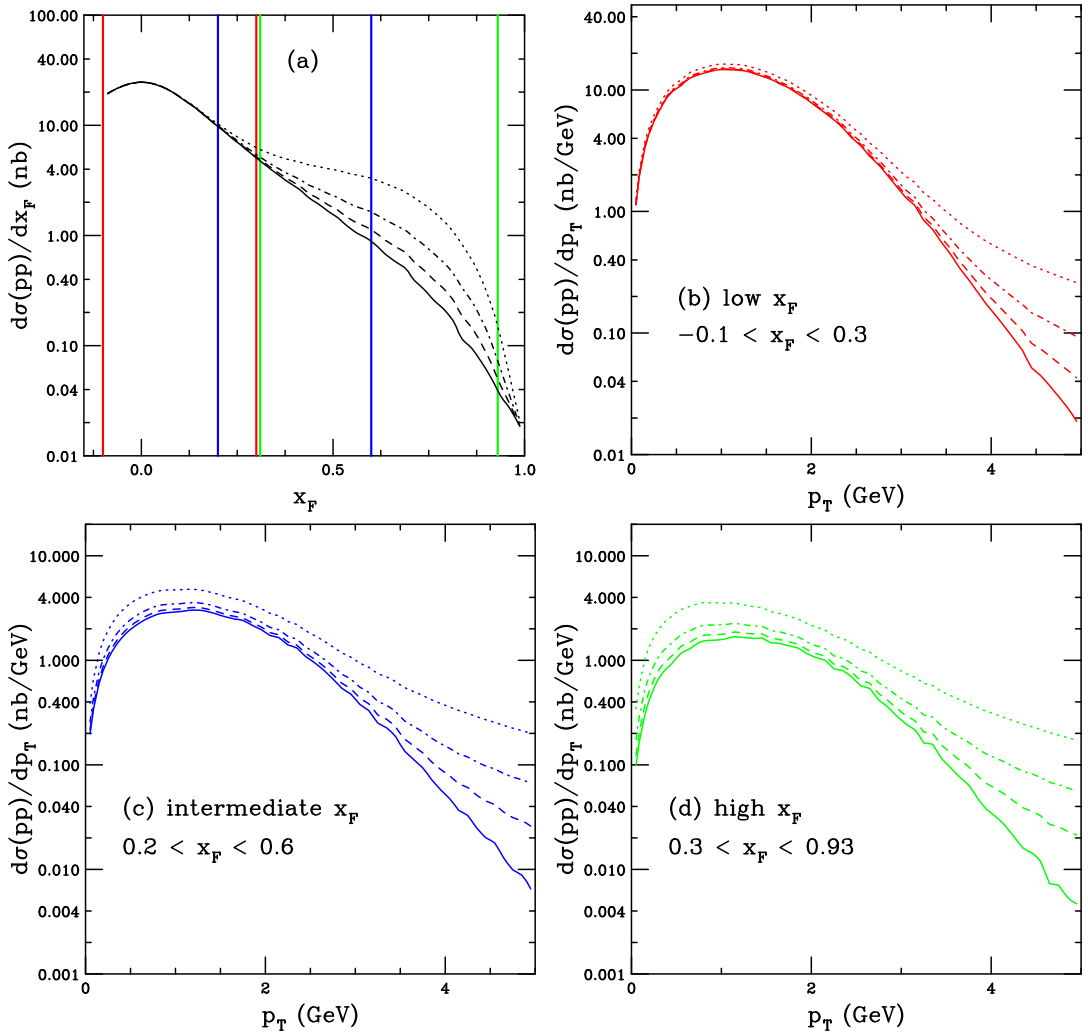

Figure 17: The J/ψ cross sections in $p+p$ collisions at $\sqrt{s} = 38.8$ GeV with and without IC as a function of x_F (a) and p_T at low (b), intermediate (c), and high x_F (d). The solid curves do not include IC while the dashed, dot-dashed and dotted curves use $P^0_{\mathrm{ic}\,5} = 0.1\%$, 0.31% and 1% respectively. The colored vertical bars on the x_F distributions show the x_F limits of the p_T distributions in (b)-(d) and matches the color of the curves in (b)-(d). RV, PRC **103**, 035204 (2021).

Comparison with α Extracted from E866 J/ψ $p+A$ Data

E866 obained α as a function of x_F and p_T (in 3 x_F bins) from Be, Fe, and W targets

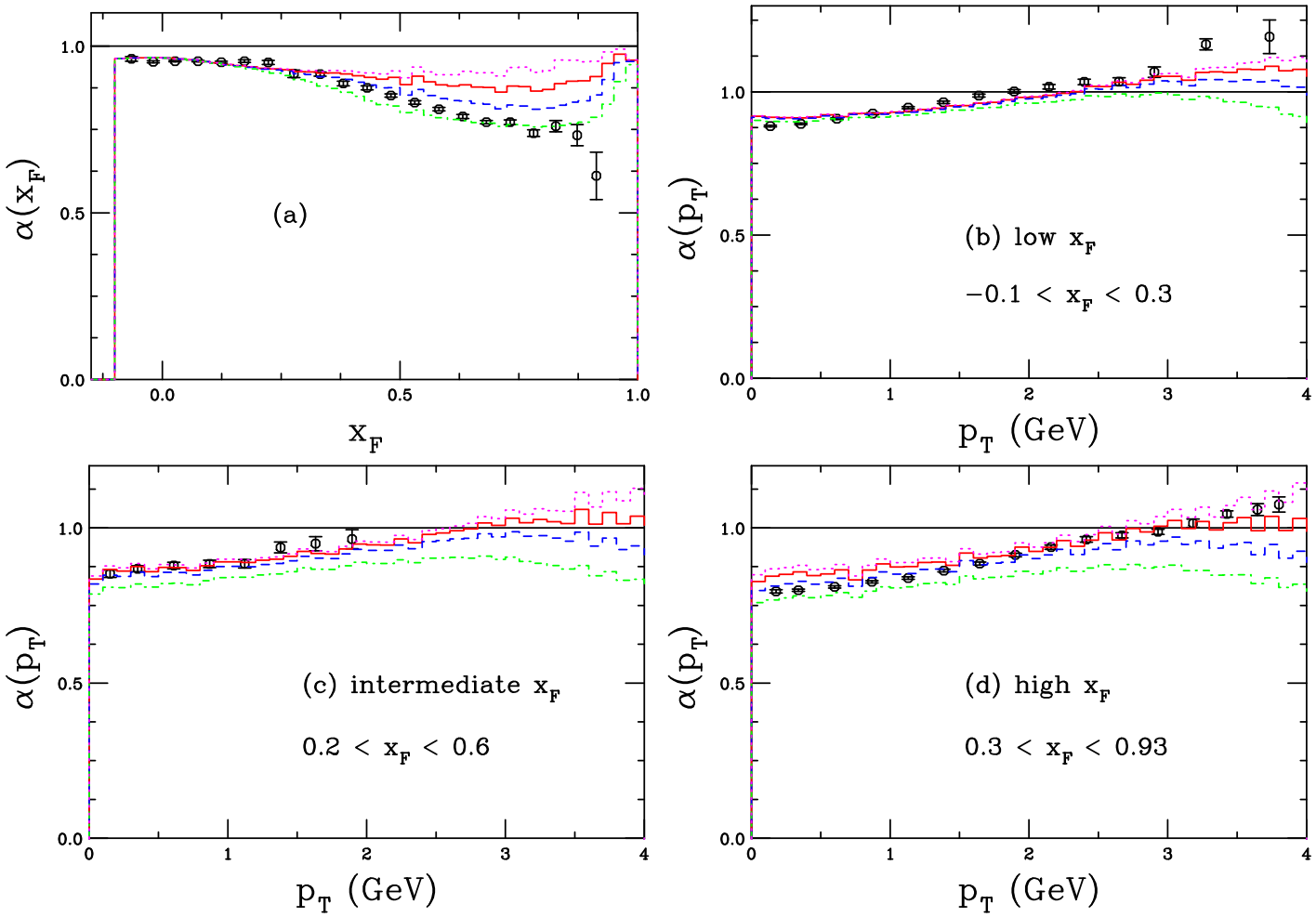

Figure 18: The exponent $\alpha(x_F)$ (a) and $\alpha(p_T)$ for low x_F (b), intermediate x_F (c), and high x_F (d). The dotted magenda curves use $P^0_{\rm ic\,5} = 0$ while the solid red, dashed blue, and dot-dashed green curves show $P^0_{\rm ic\,5} = 0.1\%$, 0.31% and 1% respectively. The E866 data (PRL **84**, 3256 (2000)) are the black points. From: RV, PRC **103**, 035204 (2021).

Comparison to $\alpha(x_F)$ from Fixed-Target J/ψ Data

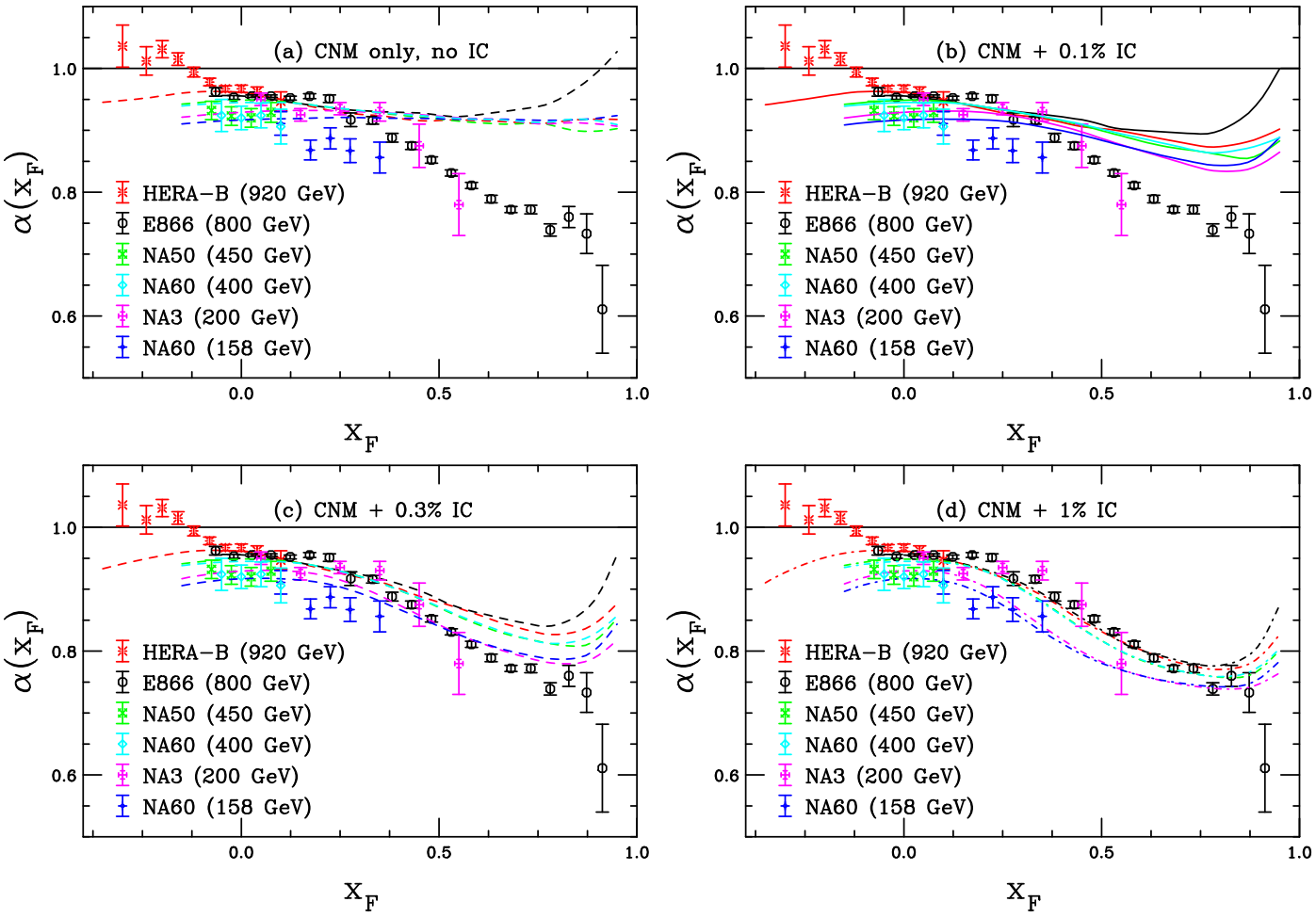

Figure 19: The value of $\alpha(x_F)$ for J/ψ production at: NA60 ($p_{\rm lab} = 158$ GeV), NA3 ($p_{\rm lab} = 200$ GeV), NA60 ($p_{\rm lab} = 400$ GeV), NA50 ($p_{\rm lab} = 450$ GeV), E866 ($p_{\rm lab} = 800$ GeV), and HERA-B ($p_{\rm lab} = 920$ GeV). The points and curves of the same color are at the same energy. Calculations with $P^0_{\rm ic\,5} = 0$ are in (a) while $P^0_{\rm ic\,5} = 0.1\%$, 0.3%, and 1% are shown in (b)-(d).

SMOG J/ψ Results for $\sqrt{s_{NN}} = 69$ GeV $p + \mathrm{Ne}$ Data

Preliminary SMOG J/ψ data shown at QM2022, with a paper in preparation

SMOG has previously published [Phys. Rev. Lett. 122, 132002 (2019)] data for $p + \mathrm{He}$ at $\sqrt{s_{NN}} = 87.7$ GeV and $p + \mathrm{Ar}$ at $sqrts_{NN} = 110.4$ GeV, both for J/ψ and for D mesons

Calculations are in progress to compare with these data, as well as expected data on D & $\overline{D}$ asymmetries which should be non-zero if intrinsic charm is significant: $\overline{D}$ can be produced from a $|uudc\bar{c}\rangle$ state while D cannot – $\overline{D}$ is leading charm while D is nonleading

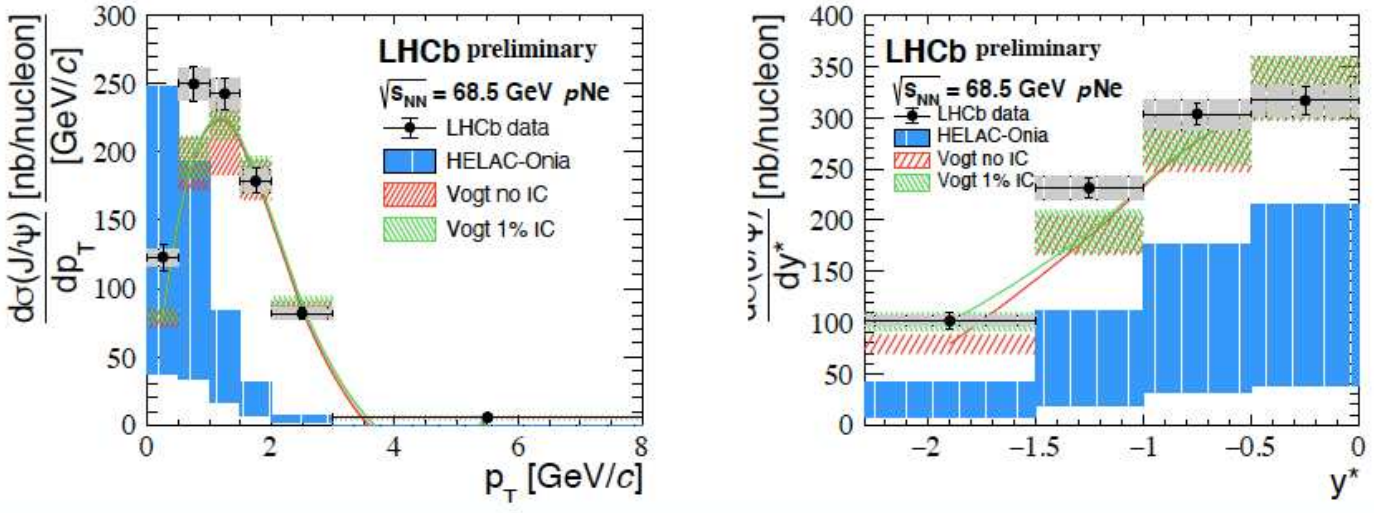

Figure 20: SMOG $p+\mathrm{Ne}$ data at $\sqrt{s_{NN}} = 69$ GeV compared to this model and HELAC-ONIA. The agreement with this model is very good but the data cannot distinguish the presence or absence of intrinsic charm to any significance.

Summary

Intrinsic charm can play a role in forward charm production at the EIC – results shown here for $p+p$ and $p+\mathrm{Pb}$ but the general argument holds for $e+p$ and $e+A$

We can perform similar calculations for EIC using the Improved Color Evaporation Model, see the next talk by Vincent

The same formalism is being applied to J/ψ and D^0 production with the fixed-target SMOG device for LHCb, as shown for the $p+\mathrm{Ne}$ data, results for other SMOG energies in progress